Theoretical and Applied Fracture Mechanics 130 (2024) 104326

Contents lists available at ScienceDirect

Theoretical and Applied Fracture Mechanics

journal homepage: www.elsevier.com/locate/tafmec

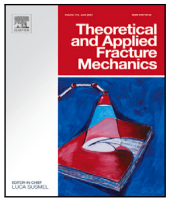

Modification of nominal strength scaling laws to pseudo-ductility

A. Subramani, P. Maimí *, J. Costa

AMADE, Escola Politecnica Superior, Universitat de Girona, Girona, 17071, Spain

ARTICLE INFO

Keywords:
Stress concentration factor
Pseudo-ductility
Nominal strength
Numerical analysis

ABSTRACT

We investigate the influence pseudo-ductility has on the notched strength and size-effect behaviour of typical notched specimens of quasi-isotropic pseudo-ductile composite materials. Our previous findings reveal that pseudo-ductility enhances translaminar toughness and nominal strength recovery but can negatively affect specimens below a critical notch size. The traditional Bažant Size Effect Law (SEL) does not adequately capture these observations, necessitating modifications to account for the non-recoverable pseudo-ductile damage past the pseudo-yield strength. We propose modifications to the nominal strength scaling laws, aiming to characterise both the notched strengths for a given notch radius and the size effect due to pseudo-ductility. Modifications are applied to centre-cracked (CC), elliptical hole (EH), and open-hole (OH) specimens for a wide range of pseudo-ductile materials. The proposed modifications for nominal strength predictions agree with FE estimates across all three notch shapes (CC, EH, and OH). The findings suggest that the presented SEL serves as a valuable tool for understanding and assessing the size-effect behaviour of pseudo-ductile composites.

1. Introduction

Quasi-brittle materials exhibit notch sensitivity, wherein the presence of notches drastically reduces the structural strength compared to its un-notched counterpart [1–3]. Furthermore, holes or cut-outs provoke a failure mode transition from ductile to brittle (embrittlement) when geometrically similar structures are scaled — a phenomenon referred to as the size effect. Fig. 1 depicts two distinct size-effect manifestations typically observed. The first behaviour (Fig. 1a) consists of a decreasing notched strength with scaling up of the specimen while maintaining constant material properties and geometric ratios, as per nominal strength scaling laws [4–7]. Conversely, the second type (Fig. 1b) involves a reduction in notched strength as the ratio of notch radius (R) to specimen width (W) increases (R/W) while maintaining constant material properties [8,9]. Traditional failure theories (e.g., maximum shear stress theory or the von-Mises yield criterion) fall short in capturing size-effect behaviour because, as they rely solely on continuum material properties, they predict a constant strength irrespective of specimen size, i.e., $\sigma_N(\text{size}) = \text{constant}$.

Thin-ply composites are becoming increasingly favoured thanks to the benefits they offer such as minimised manufacturing defects, enhanced free-edge delamination resistance, and lower statistical variation in material properties [10–12]. Nonetheless, these materials have one notable drawback: increased brittleness, due to the reduction of sub-critical damage mechanisms (for e.g.matrix cracking) which provide stress relief to the stress risers. Pseudo-ductility, introduced through ply-level hybridisation (typically alternating high and low failure strain thin plies), aims to counteract this [13–17]. By fostering sub-critical damage mechanisms – fibre or ply fragmentation, dispersed delamination, and eventual saturation – pseudo-ductility aspires to emulate a "metal-like" stress–strain behaviour (Fig. 2a) [14–17]. Achieving such a response is expected to reduce the stress concentration factor (K_t) by facilitating the redistribution of elevated stresses around the notch [9,18–20].

In previous research, we used a user-defined material model representative of idealised pseudo-ductility (Fig. 2a) to numerically assess the effect of pseudo-ductility on both translaminar toughness ($\mathcal{G}_{I_c}$) and the stress-concentration factor (K_t), or notched strength, σ_N [21,22]. The compact-tension (CT) models demonstrated that pseudo-ductility augments the $\mathcal{G}_{I_c}$. Furthermore, pseudo-ductility was found to enhance the recovery of nominal strength in typical notched specimens, attributable to concurrent improvements in K_t and $\mathcal{G}_{I_c}$. While pseudo-ductility benefits larger specimens, it was detrimental for specimens below a critical notch size [21,22] as the Bažant Size Effect Law (SEL) did not adequately capture the size effect behaviour of these specimens, despite considering the modified $\mathcal{G}_{I_c}$ and K_t [21,22]. We hypothesise that this limitation arises from neglecting the non-recoverable pseudo-ductile damage (Fig. 2b) when the average stresses (σ_N) in the failure plane exceed the pseudo-yield strength (σ_y). To rectify this, we intend to modify the nominal strength scaling laws to account for the pseudo-ductile damage, drawing inspiration from the work of Stowell [23] and Hardarth [24].

* Corresponding author.
E-mail address: pere.maimi@udg.edu (P. Maimí).

https://doi.org/10.1016/j.tafmec.2024.104326
Received 10 November 2023; Received in revised form 18 January 2024; Accepted 14 February 2024
Available online 20 February 2024

Symbol	Description
b	Semi-minor notch radius
t	Specimen thickness
h	Modulus ratio, H/E
A	Net-section area, $(W-R)t$
E	Young's modulus
E_S	Secant modulus
F	Finite width correction factor
F_u	Peak-load carried by the notched specimen
H	"Hardening" modulus
R	Notch radius
$2W$	Specimen width
ε_y	Pseudo-yield strain
ε_f	Failure or ultimate strain
ε_d	Pseudo-ductile strain
e_d	Strain-ratio, $\varepsilon_d/\varepsilon_y$
σ_y	Pseudo-yield stress
σ_f	Failure stress or un-notched strength
σ_N	Nominal strength F_u/A
σ_∞	Gross strength F_u/Wt
s_H	Strength-ratio, σ_f/σ_y
s_N	Normalised nominal strength σ_N/σ_f
$\mathcal{G}_{Ic}$	Translaminar fracture toughness
$\mathcal{J}^{SS}$	Translaminar fracture toughness of a pseudo-ductile material
$\bar{\mathcal{J}}^{SS}$	Translaminar toughness ratio, $\mathcal{J}^{SS}/\mathcal{G}_{Ic}$
Π_N	Neuber non-dimensional Π-group, e_d/s_H
K_t^E	Elastic stress concentration factor, Net
K_{tg}	Elastic stress concentration factor, Gross, $K_t^E(1-R/W)^{-1}$
K_t^P	Pseudo-ductile stress concentration factor
K_t^M	Modified pseudo-ductile stress concentration factor
ℓ_{FPZ}	Failure process zone length
ℓ_M	Material characteristic length or Irwin length, $E\mathcal{J}^{SS}/\sigma_f^2$
ℓ_{SEL}	Size effect length, $\ell_M/(\pi F^2)$
$\bar{\ell}_M$	Normalised ℓ_M, ℓ_M/R
$\bar{\ell}_{\text{SEL}}$	Normalised ℓ_{SEL}, ℓ_{SEL}/R
$\bar{\ell}_{\text{SEL}^*}$	Normalised piecewise pseudo-ductile size effect length

Through the proposed modifications, this work aims to quickly characterise the notched strengths or size-effect laws of typical notches for an ideally pseudo-ductile material. The article is structured as follows: Section 2 offers a brief introduction to the nominal strength scaling laws. Drawing from the insights of [23–25], modifications to the nominal strength scaling laws are introduced considering typical notches in Section 2.1. The third section, Section 3, offers a concise overview of the material model, non-dimensional analysis, and Design of Experiments (DOE) that we used to validate the presented modifications and their capacity to predict the nominal strength. Results of the altered scaling laws are compared against the nominal strength of a pseudo-ductile material with a centre-crack (CC), an elliptical hole (EH), and an open hole (OH) (Sections 5.1 and 5.2). The universality of the updated scaling laws across diverse pseudo-ductile materials is also discussed and validated. Concluding in Section 5.3, we leverage the modified nominal strength scaling laws and the functional form to discern general nominal strength behaviours of pseudo-ductile materials across a broad range, from low to high pseudo-ductility.

2. Nominal strength scaling laws

Failure strength of notched specimens is generally defined as the mean stress in the failure plane just before failure. Two commonly used measures to define notched strength are nominal and gross stress, representing the mean stress in the net-section (plane a-b in Fig. 1b inset) and gross-section (plane c-d in Fig. 1b inset), respectively. Assuming a net-section failure with F_u being the peak load, the nominal strength (σ_N) of a notched structure is given by,

$$\sigma_N = \frac{F_u}{2(W-R)t} \tag{1}$$

where, $2(W-R)t$ is the net-section area. The far-field or gross-strength (σ_∞) can be related with the nominal strength in Eq. (1) through,

$$\sigma_\infty = \sigma_N\left(1-\frac{R}{W}\right) \tag{2}$$

The first manifestation of notch embrittlement (Fig. 1a), generally known as the scaling law, is determined by asymptotically matching the small size ($R\to 0$) and large size ($R\to\infty$) asymptotic expansions [1]. Note that, in large specimen sizes, width and notch size distinctions become insignificant. The σ_N of the smaller specimens – notch independent – follow the plastic limit theory, $\lim_{R\to 0}\sigma_N = \sigma_f$. Whereas, the σ_N of the larger specimens are notch-dependent and follows the elastic limit theory, according to $\lim_{R\to\infty}\sigma_N = \left(\sigma_f/K_t\right)$ for EH and OH, $\lim_{R\to\infty}\sigma_N = \left(\bar{\ell}_{\text{SEL}}\right)^{1/2}$ for CC, where $\bar{\ell}_{\text{SEL}}$ is the normalised failure process zone length (ℓ_{FPZ}/R), Eq. (4). Quasi-brittle materials are known to develop a finite length FPZ before failure [4,5]. This can be thought of as relieving the stress concentration, having a similar effect as in plastic materials [26]. The relative length of the failure process zone changes with the specimen size, resulting in the observed transition from a ductile to a brittle failure mode with increasing specimen sizes. The material characteristic length ℓ_M, introduced by Irwin [27], captures the ℓ_{FPZ} well. The SEL, in general form, is given by [28],

$$s_N = \frac{\sigma_N}{\sigma_f} = \left(\frac{K_t^{-r}+\bar{\ell}_{\text{SEL}}}{1+\bar{\ell}_{\text{SEL}}}\right)^{\frac{1}{r}} \tag{3}$$

where K_t is the stress concentration factor, as detailed in Appendix A, for a given notch.

$$\bar{\ell}_{\text{SEL}} = \frac{\ell_{\text{SEL}}}{R} = \frac{\ell_M}{\pi R F^2} = \frac{E\mathcal{G}_{Ic}}{\pi R F^2\sigma_f^2} \tag{4}$$

where $\ell_M(=E\mathcal{G}_{Ic}/\sigma_f^2)$ is the material characteristic length or Irwin length, a material property related to the translaminar fracture toughness, elastic modulus, and the un-notched strength. F is the geometric correction factor to account for the finite geometric effects [29], given by Eq. (B.1). The parameter r in Eq. (3), typically seen as a fitting variable [7,28], is set to 2 for fracture mechanics specimens like CC, consistent with LEFM. Whereas, for other types of notches the value is typically less than 2, and is usually determined through fitting experimental data [7,28].

Another widely known size-effect phenomenon is the decrease of notched strength with the increase of notch size ratio (R/W) [8,30], Fig. 1b. Depending on the material's stress redistribution capability, notched strength can fall between the un-notched strength (notch-insensitive) and the completely notch-sensitive strength (σ_f/K_{tg}) – K_{tg} is the gross-stress concentration factor, see Appendix A. This is further complicated in quasi-brittle composite materials as, depending on the R/W ratio, they tend to exhibit both the extremes. When the notch ratio is relatively small ($R/W\to 0$), composites are completely notch-insensitive. Conversely, they become completely notch-sensitive towards the other extreme ($R/W\to 1$) due to the increased K_{tg} influence from the notch (K_{tg} increases with increasing R/W, see Eq. (A.3)).

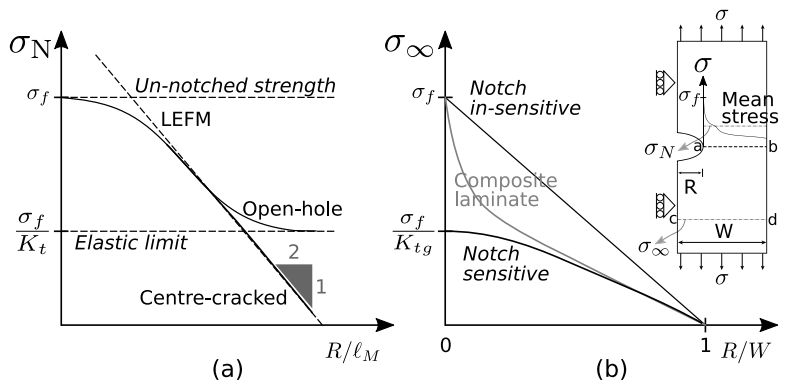

Fig. 1. Dependence of notched strength on geometric and material parameters for quasi-brittle materials. (a) Size effect behaviour on notched strength (b) Limits of notch sensitivity. Here, R/W is the ratio of notch-radius to specimen half-width and R/ℓ_M is the normalised material characteristic length, where $\ell_M = E\mathcal{G}_{Ic}/\sigma_f^2$.

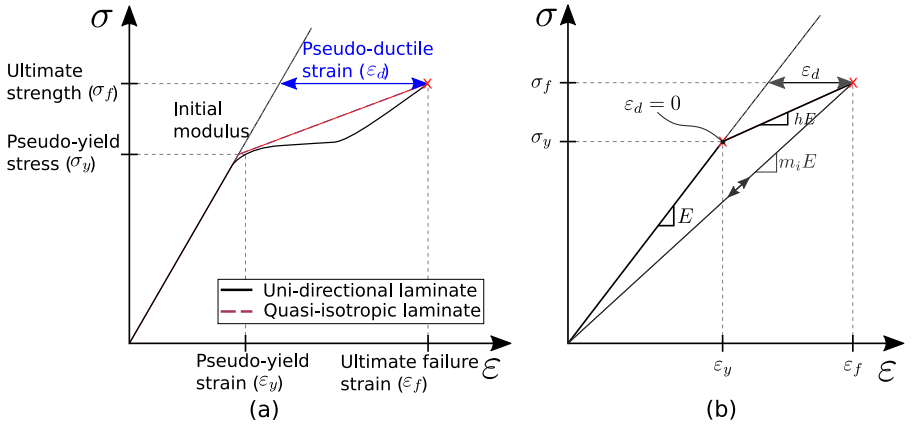

Fig. 2. Description of (a) representative uni-axial tensile response of unidirectional and quasi-isotropic pseudo-ductile composite laminates and (b) pseudo-ductile constitutive behaviour. The modulus ratio, $h \in [0, 1]$; $h = 1$ and 0 represent a linear-elastic and a perfectly plastic material, respectively.

2.1. Modified nominal strength scaling laws

The Bažant SEL in Eq. (3) is derived for quasi-brittle materials [28], considering the extreme ratios of Failure Process Zone (FPZ) length (ℓ_{FPZ}) to specimen width (W), represented as ℓ_{FPZ}/W. Despite accounting for the increased fracture energy ($\mathcal{G}_{Ic}$) and decreased stress concentration factor (K_t^P) associated with pseudo-ductility, we still observe that SEL overestimates the nominal strengths in the region where $\sigma_N > \sigma_y$ [21,22]. We hypothesise that the overestimation is partially due to not accounting for the stiffness change associated with pseudo-ductile damage mechanisms after "yielding".

Utilising continuum damage mechanics principles [31], a damaged material can be regarded as an effective material with reduced stiffness. Consequently, substituting the constant elastic modulus in Eq. (3) with a stress-dependent secant modulus, $E_S(\sigma)$, provides a simplistic yet remarkably effective approach to account for the pseudo-ductile damage. For any given stress, the secant modulus, E_S, can be expressed as,

$$E_S(\sigma_i) = \frac{\sigma_i}{\varepsilon_i} \tag{5}$$

where σ_i and ε_i are the stress and strain, respectively. For the idealised pseudo-ductile material following Fig. 2b, the secant modulus prior to material failure ($\sigma < \sigma_f$) is,

$$E_S = \begin{cases} E, & \sigma_i < \sigma_y \\ \frac{\sigma_i hE}{\sigma_i - \sigma_y(1-h)}, & \sigma_y < \sigma_i < \sigma_f \end{cases} \tag{6}$$

where, $h = H/E$ represent the "hardening" to elastic modulus ratio, see Fig. 2b. Thus, the secant modulus at the nominal strength (though unknown) is,

$$E_S = \frac{\sigma_N hE}{\sigma_N - \sigma_y(1-h)} \tag{7}$$

Therefore, by substituting Eq. (6) in Eq. (4), the modified $\bar{\ell}_{\text{SEL}}$ for a pseudo-ductile material can be presented as,

$$\bar{\ell}_{\text{SEL}^*} = \begin{cases} \bar{\ell}_{\text{SEL}} & \text{for } s_N < 1/s_H \\ \bar{\ell}_{\text{SEL}} \left(\frac{s_N h}{s_N - (1-h)/s_H} \right) & \text{for } 1/s_H < s_N < 1 \end{cases} \tag{8}$$

where $s_H = (\sigma_f/\sigma_y)$ represent the ratio of un-notched (σ_f) to pseudo-yield strength (σ_y), see Fig. 2b. We begin by addressing the scaling law of a pseudo-ductile CC notch because it is straightforward (Section 2.1.1), and then subsequently move on to other notch shapes (EH and OH), Section 2.1.2.

2.1.1. Centre-cracked specimens

In this article, we make use of the pseudo-ductility modified translaminar toughness ($\mathcal{J}^{SS}$) for pseudo-ductile materials [21]. Hence, by virtue of LEFM, the elastic limit of a pseudo-ductile material can be determined by substituting the corresponding translaminar toughness, i.e., replacing $\mathcal{G}_{Ic}$ with $\mathcal{J}^{SS}$. Thus, for a centre-cracked specimen ($K_t \to \infty, R \to \infty$), the strength limit is reached, when,

$$s_N = \sqrt{\bar{\ell}_{\text{SEL}}} = \sqrt{\frac{\ell_M}{\pi RF^2}} = \sqrt{\frac{E\mathcal{J}^{SS}}{\pi RF^2\sigma_f^2}} \tag{9}$$

To incorporate the aforementioned stiffness reduction due to pseudo-ductility, $\bar{\ell}_{\text{SEL}}$ should be substituted by $\bar{\ell}_{\text{SEL}^*}$ in Bažant SEL (i.e., Eq. (8)

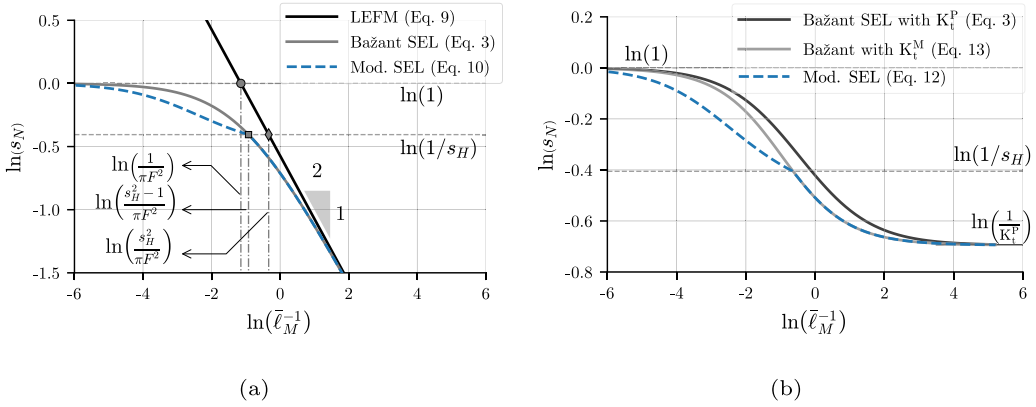

Fig. 3. Proposed s_N modifications for a centre-cracked and an open-hole specimen of pseudo-ductile material ($\Pi_N/h = 10, s_H = 1.5, h = 0.1$). Note that the y-axis scales are different between (a) and (b). In $\bar{\ell}_M$, the translaminar toughness, $\mathcal{G}_{I_c}$, is used instead of the $\mathcal{J}^{ss}$, for the linear-elastic material.

in Eq. (3) with $r = 2$, $K_t \to \infty$). Although an explicit function for $s_N\left(\bar{\ell}_{\text{SEL}}\right)$ exists – see Appendix D – it is convenient to express it using its inverse as,

$$\bar{\ell}^{-1}_{\text{SEL}} = \begin{cases} \frac{1-s_N^2}{s_N^2} & \text{for } s_N < 1/s_H \\ \frac{1-s_N^2}{s_N}\frac{h}{s_N-(1-h)/s_H} & \text{for } 1/s_H < s_N < 1 \end{cases} \tag{10}$$

To better comprehend the presented modifications, we display the nominal strengths derived from the modified equations (Eq. (10)) together with their linear-elastic counterparts (Eqs. (3) and (9)) in Fig. 3. This analysis assumes an arbitrary pseudo-ductile material characterised by $h = 0.1$ and $s_H = 1.5$. The nominal strengths are presented in a non-dimensional form in Fig. 3a, for $\bar{\ell}_{\text{M}}\left(\ell_{\text{M}}/R\right)$ values ranging from 10^{-3} to 10^{3}.

Several characteristic features of Eq. (10) are evident in Fig. 3a. Firstly, the root (circular marker) of the plastic limit theory (with unnotched strength, $s_N = 1$) and LEFM (Eq. (9)) aligns with $1/(\pi F^2)$ as in [7]. This observation suggests that it is reasonable that the modifications to the LEFM (Eq. (D.5)) should coincide with $s_H^2/(\pi F^2)$ when s_N is $1/s_H$ (diamond marker). Furthermore, an additional root can be derived to be at $(s_H^2 - 1)/\pi F^2$ between SEL (Eq. (3)) and its modified counterpart (Eq. (10)), with $s_N = 1/s_H$ (square marker). This root corresponds to the notch size threshold below which the pseudo-ductile damage can be considered to accurately characterise the nominal strength.

2.1.2. Elliptical or open-hole specimens

We extend the methodology used for CC specimens (Section 2.1.1) to EH and OH notches. Consequently, using the modified FPZ length (Eq. (8)), one can express the modified SEL in a generic form as,

$$s_N = \left[\frac{\left(K_t^P\right)^{-r} + \bar{\ell}_{\text{SEL}^*}}{1 + \bar{\ell}_{\text{SEL}^*}}\right]^{\frac{1}{r}} \tag{11}$$

where K_t^P is the pseudo-ductile stress concentration factor. Substituting the corresponding values of $\bar{\ell}_{\text{SEL}^*}$ and expressing s_N via its inverse, for convenience, results in,

$$\bar{\ell}^{-1}_{\text{SEL}} = \begin{cases} \frac{1-s_N^r}{s_N^r-\left(K_t^M\right)^{-r}} & \text{for } s_N < 1/s_H \\ \frac{1-s_N^r}{s_N^r-\left(K_t^M\right)^{-r}}\frac{hs_N}{s_N-(1-h)/s_H} & \text{for } 1/s_H < s_N < 1 \end{cases} \tag{12}$$

where the plastic stress concentration factor, K_t^P, is modified to K_t^M such that $\lim_{R\to\infty} K_t^M = K_t^P$ to guarantee the correct asymptotic elastic limit ($s_N = 1/K_t^P$), defined as,

$$K_t^M = \frac{K_t^P - 1}{1 - s_N} \tag{13}$$

In Fig. 3b, we demonstrate the characteristics of the proposed modifications using an OH for the same arbitrary pseudo-ductile material considered earlier, with $h = 0.1$, $s_H = 1.5$, and $e_d/s_H = 1$, for $\bar{\ell}_{\text{M}}$ values ranging from 10^{-3} to 10^{3}. This material results in a K_t^P of 2 (using the modified Stowell model from [22] and Section 4.2) and the $K_t^E = 3$ for an OH (Appendix A). Fig. 3b also compares s_N predictions with (grey line) and without (black line) K_t^M modifications.

3. Methodology

Previously [21], we developed a user-defined material model to characterise pseudo-ductility (Fig. 2b) under plane-stress loading conditions. By considering pseudo-ductile laminates on a macro-scale (homogenised laminate) level, we characterised the influence of pseudo-ductility on translaminar toughness and nominal strengths of notched specimens [21,22]. In this work, a similar methodology is used to validate the modified nominal strength scaling laws (Section 2.1) through finite element (FE) models.

In a macro-scale modelling approach, the entire laminate is homogenised with equivalent properties to characterise the constitutive behaviour [31]. We chose this approach to eliminate the need for intricate details of the laminate necessary to achieve successful pseudo-ductility, e.g., the thickness and elastic modulus of low and high strain plies. Using macro-scale modelling also reduces the number of variables that must otherwise be considered in the design of experiments (DOE). Two constitutive models come into play: a cohesive element defining the fracture plane (characterised by σ_f and $\mathcal{G}_{I_c}$) and a user-defined constitutive model of pseudo-ductility describing continuum elements elsewhere. Briefly, the constitutive behaviour is characterised by a principal failure strain criterion to capture damage initiation. Material degradation beyond the failure strength (σ_f) is not implemented since the cohesive elements are placed in series. Thus, at σ_f, the crack begins to propagate.

Following [32,33], the normalised nominal strength (s_N) of any notched pseudo-ductile structure takes this form [22],

$$s_N = f_u\left(\varepsilon_d, s_H, \frac{\ell_M}{R}, \frac{b}{R}, \frac{R}{W}\right) \tag{14}$$

where $\varepsilon_d (= \varepsilon_f - \sigma_f/E)$ is the pseudo-ductile strain at failure, $s_H (= \sigma_f/\sigma_y)$ represents the strength ratio, R/W is the notch radius to width ratio, $\ell_M/R (= \bar{\ell}_{\text{M}})$ is the normalised material characteristic length and b/R is the ratio of notch radius between semi-minor and semi-major axis.

We have examined the dependency of s_N, as expressed in Eq. (14), on material parameters (ε_d, s_H) and geometric factors $(R, b/R, R/W)$ through a two-pronged DOE approach. Adopting a 'one factor at a time' method, the material parameters (ε_d, s_H) are considered first. Here, we considered a quasi-isotropic pseudo-ductile material with four distinct

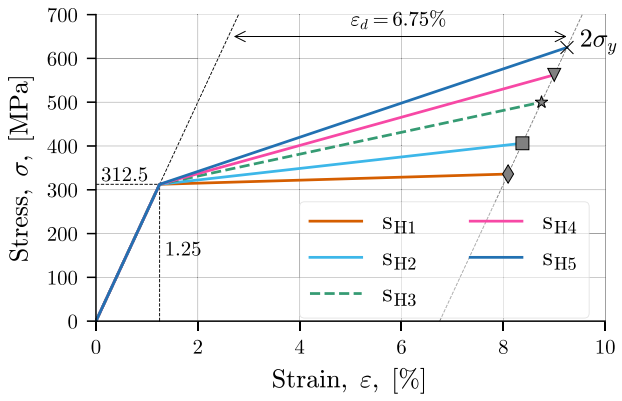

Fig. 4. Design of experiments (ε_{di} study) for the uni-axial pseudo-ductile stress–strain response. Only ε_d of 6.75% is shown but ε_d = 0.5, 1.2 and 2.85% is considered in the parametric study. $s_{Hi} = \sigma_f/\sigma_y$ range from 1.075, 1.3, 1.6, 1.8, and 2.0.

ε_d values, logarithmically increasing from 0.5 to 6.75% (ε_d = 0.5, 1.2, 2.85, and 6.75%), and five different strength ratios (s_H = 1.075, 1.3, 1.6, 1.8, and 2.0), as seen in Fig. 4. This resulted in a total of 20 unique pseudo-ductile materials. Further, a linear elastic material (E = 25 GPa, ε_f = 2%, $\mathcal{G}_{Ic}$ = 75 N mm^{-1}) is included for validation. As the influence of yield strain is typically disregarded [21,32,34], it is taken a constant value of ε_y = 1.25%.

Eq. (14) evidences three geometric dependencies on nominal strength. Firstly, for the geometric/notch shape dependency, b/R, we consider values of ≈0, 0.5, and 1 to represent CC, EH, and OH notch shapes, respectively. Regarding the notch size ratio, R/W, we chose a constant value of 1/6. Note that, as its influence on s_N is through F and K_t, other R/W could be characterised by considering appropriate F and K_t values. Lastly, for the size dependency, ℓ_M, scaled size-effect models with R ranging from 0.1 to 160 mm are taken into account. Fig. 5 shows the two-dimensional half-symmetric plane-stress models containing the CC, EH, and OH notches and their associated boundary conditions.

In addition, we conducted a further DOE to investigate how pseudo-ductility influences the s_N with the changing notch ratios (R/W), as depicted in Fig. 1b. Four distinct FE models featuring an OH notch were constructed for this investigation. These models, representing both an elastic and a pseudo-ductile material, had a constant specimen width (W = 50 mm) but varied in their R/W ratios (0.1, 0.2, 0.3, and 0.4).

4. Translaminar toughness and stress concentration factor of pseudo-ductile materials

As pseudo-ductility influences the translaminar fracture toughness ($\mathcal{J}^{SS}$) and the stress concentration factor (K_t) [21,22], it is necessary to quickly determine the $\mathcal{J}^{SS}$ and K_t to characterise the nominal strength of any notched structure. Within the context of the current work, we directly examine the previous results and present the relevant aspects from [21,22].

4.1. Translaminar fracture toughness

Previously, we used half-symmetric plane-stress CT FE models to determine the increment of translaminar toughness due to pseudo-ductility [21]. Non-dimensional analysis revealed that the steady-state crack propagation in a pseudo-ductile material (following Fig. 2b) could adequately be characterised by [21],

$$\bar{\mathcal{J}}^{SS} = \frac{\mathcal{J}^{SS}}{\mathcal{G}_{Ic}} = f_{ss}\left(\varepsilon_y, \varepsilon_d, s_H\right) \tag{15}$$

The pseudo-yield strain (ε_y) was eliminated from Eq. (15), as its influence is deemed negligible [32,34] and we also confirmed its negligible influence in [21]. A reasonable functional form (inspired by [35]) that describes the relationship between the normalised translaminar toughness and the non-dimensional variables ε_d and s_H is given by,

$$\bar{\mathcal{J}}^{SS} \approx 1 + B\varepsilon_d \left[\frac{s_H - 1}{s_H^a}\right] \tag{16}$$

where B and a are fitting coefficients. Based on the FE results [21], for the same material DOE (Fig. 4), coefficients of B and a are 25.776 and 2.105, respectively (See Appendix C for detailed information). Despite the potential circular reasoning, we have observed a strong correlation between the predictions (Eq. (16)) and the FE results [21], as shown in Fig. 6 — correlation coefficient (R^2) of 0.98.

Another approximation to the normalised fracture toughness could be obtained by adapting Zehnder et al. [35] models to the linear pseudo-plastic materials (see Appendix C), resulting in,

$$\bar{\mathcal{J}}^{SS} = 1 + \frac{1}{2\pi}\left(\frac{1}{h} - 1\right)\left[\frac{s_H - 1}{s_H^2}\right] = 1 + \frac{\varepsilon_d}{2\pi s_H^2 \varepsilon_y} \tag{17}$$

From Eq. (16), it is apparent that when $s_H = 1$, $\mathcal{J}^{SS}$ experiences no enhancement because the damage is likely to be confined to a plane. Contrarily, Eq. (17) indicates a minor enhancement. Additionally, while Eq. (17) implies a correlation with ε_y, numerical results reveal no significant influence [21,34].

4.2. Pseudo-ductile stress concentration factor

In an earlier work, [22], analytical models were used to characterise the stress concentration factor K_t for pseudo-ductile materials. As s_N characterisation (Eqs. (3) and (11)) requires K_t, we briefly explain our approach from [22] here for completeness. Following Stowell [23] and Hardarth [36], the plastic stress concentration for any notch is given by,

$$K_t^P = 1 + \left(K_t^E - 1\right)\frac{E_S\left(\sigma_{\max}\right)}{E_S\left(\sigma_{\text{mean}}\right)} \tag{18}$$

where, $E_S(\sigma_{Max})/E_S(\sigma_{Mean})$ is the secant modulus ratio between the point of the maximum stress and the average stress in the failure plane, and K_t^E is the elastic K_t (K_t^E from handbooks [29,37] is presented in Appendix A).

For the idealised pseudo-ductile material (Fig. 2b) considered here, there exist three distinct regions of the secant modulus ratio $E_S(\sigma_{Max})/E_S(\sigma_{Mean})$, which correspond to different stress concentration factors. These regions are: the elastic region ($\sigma_{Max} < \sigma_y$), the small-scale yielding region ($\sigma_{Max} > \sigma_y$ and $\sigma_{Mean} < \sigma_y$), and the large-scale yielding region ($\sigma_{Max} > \sigma_y$ and $\sigma_{Mean} > \sigma_y$), resulting in [22],

$$K_t{}^P = \begin{cases} K_t{}^E & \text{if } \sigma_{Max} < \sigma_y \\ \frac{K_t^E + \Pi_N}{1 + \Pi_N} & \text{if } \sigma_{Max} > \sigma_y \text{ and } \sigma_{Mean} < \sigma_y \\ \frac{K_t^E - 1 + h(1+\Pi_N)}{1 + (K_t^E - 2)(1 - h(1+\Pi_N))} & \text{if } \sigma_{Mean} > \sigma_y \end{cases} \tag{19}$$

where Π_N is e_d/s_H with $e_d = (\varepsilon_d/\varepsilon_y)$. Validated by the FE models, Eq. (19) displays a good correlation (R^2) between predicted and FE results for EH and OH, 0.88 and 0.99, respectively.

5. Results

This results section uses FE models to validate the proposed modifications (Eqs. (10) and (12)) to Bažant's SEL (Eq. (3)). Our initial focus is a detailed comparison of FE results with predictions from the modified and Bažant's SELs for geometrically scaled FE models (Sections 5.1 and 5.2). These models consist of three notch shapes (CC, EH, and OH) and are made of a high pseudo-ductility material. Subsequently, we evaluate the modifications' prediction accuracy across various pseudo-ductile materials, notch shapes, and sizes. The modified SEL is used

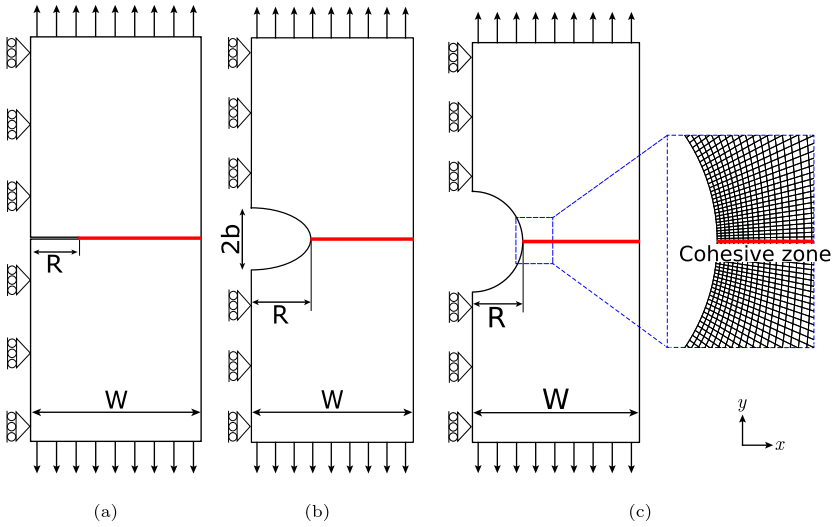

Fig. 5. Representative half-symmetric FE models of (a) centre-crack, (b) elliptical hole and (c) open hole specimens and its boundary conditions. R and W are notch radius and specimen half-width, respectively.

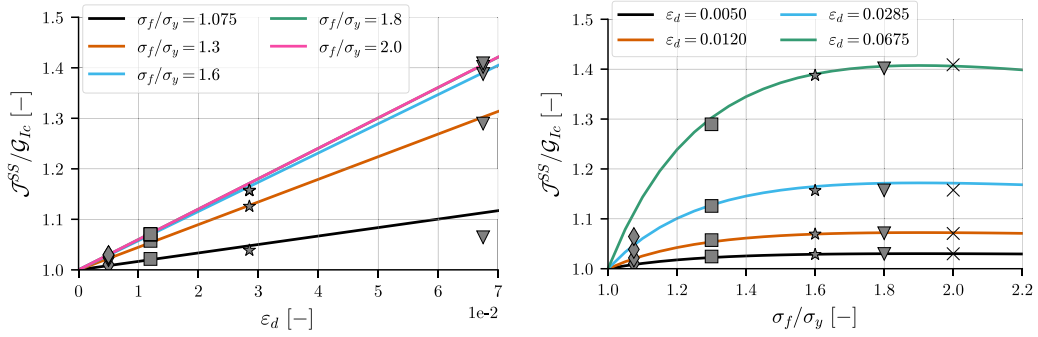

Fig. 6. Normalised steady-state energy release rate ($\bar{\mathcal{J}}^{SS} = \mathcal{J}^{SS}/\mathcal{G}_{Ic}$) for (a) increasing ε_d and (b) increasing s_H. Markers represent the FE results and the continuous lines are drawn using the functional form identified in Appendix C.

to probe the generalised s_N behaviour for all notch types (CC, EH, and OH) with an elastic material and two pseudo-ductile materials of different ductility levels (Section 5.3). Further, with the modified SEL we extend the investigation to various notch shapes with R/b ratios from 1 to ∞ (Section 5.3). The study concludes with a brief analysis of the pseudo-ductility's effect on notch-sensitivity (Section 5.4).

5.1. Nominal strength of notched pseudo-ductile specimens with centre-crack

We consider an arbitrary pseudo-ductile material with $\varepsilon_d = 6.75\%$, $\varepsilon_y = 1.25\%$, $s_H = 1.6$ and $\Pi_N/h = 33.75$. Fig. 7 shows that the strength limits align well with the expected response of a centre-cracked quasi-brittle material, i.e., $\lim_{R\to\infty} s_N = \left(\bar{\ell}_{\text{SEL}}\right)^{1/2}$, and $\lim_{R\to 0} s_N = 1$. The LEFM limit is determined by accounting for the toughness improvements due to pseudo-ductility, $\mathcal{J}^{SS}(=1.4\mathcal{G}_{Ic})$, which is calculated using the functional form in Eq. (16). For the considered pseudo-ductile material, the Bažant SEL predictions (Eq. (3)) show good agreement with both extremes of specimen size (solid line in Fig. 7) when the corresponding $\mathcal{J}^{SS}$ is used. However, below the critical specimen size – $R < \ell_{\text{SEL}}\left(s_H^2 - 1\right)$ – the agreement is poor, with nominal strength differences of up to −14%. Whereas, the nominal strengths from the proposed modifications (Eq. (10)) correlate well with the FE results for the entire range of specimen sizes (dash-dotted line in Fig. 7).

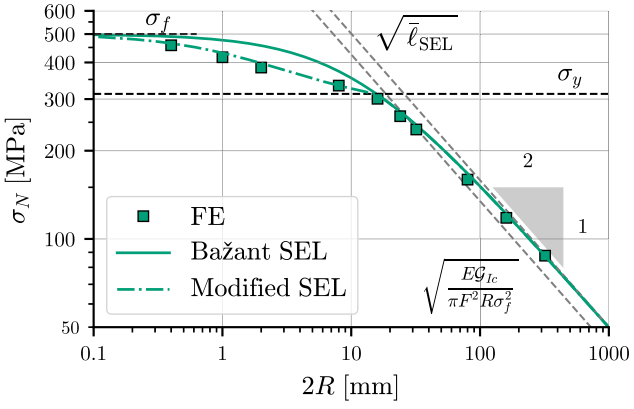

Fig. 7. Nominal strength (centre-cracked) predictions of secant modulus modified Bažant size effect law (Eq. (10)) for a pseudo-ductile material with $h = 0.1$, $s_H = 1.6$ and $\varepsilon_d = 6.75\%$.

To confirm the general applicability of these identified modifications, we use the same procedure to characterise the s_N with the FE models, for all pseudo-ductile materials considered in the DOE (Fig. 4), detailed in Appendix E. Fig. 8 reinforces the universality of these

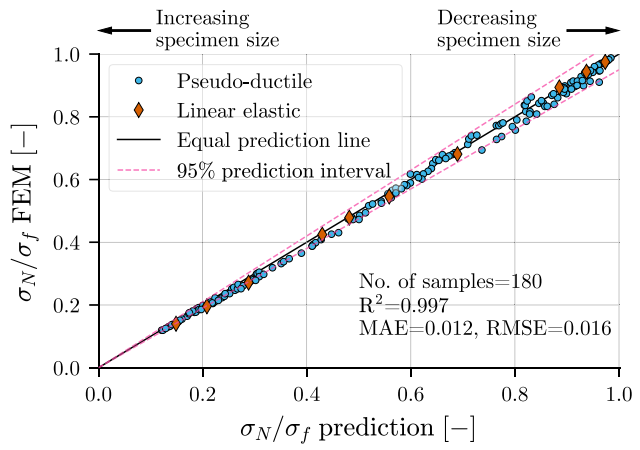

Fig. 8. Comparison of notched strengths (centre-crack) from FE models and modified nominal strength scaling laws (Section 2.1): A "1:1" correlation analysis. Markers represent FE Results (diamonds for linear-elastic, circles for pseudo-ductile).

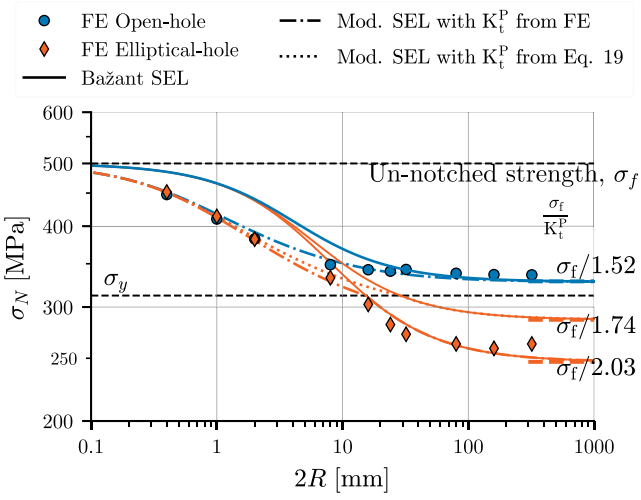

Fig. 9. Size-effect behaviour of a pseudo-material (h = 0.1, s_H = 1.6 and ε_d = 6.75%) for EH and OH notches. σ_N, is computed using the pseudo-stress concentration factor (K_t^P) derived from the modified Stowell model (Eq. (19), dotted line) and FE models (dash-dotted line). For an OH, the discrepancy between K_t^P estimates from the modified Stowell model and FE models is negligible; hence it is not depicted.

modifications, as demonstrated by the "1:1" correlation value of 0.997 (R^2) between the predicted s_N (Eq. (10)) and the FE results.

5.2. Nominal strength of notched pseudo-ductile specimens with elliptical and open-hole

Using the methodology outlined in Section 5.1, we compare the s_N from the FE models with the predictions from both Bažant's Size Effect Law (SEL, Eq. (3), solid lines) and the modified SEL (Eq. (12), dash-dotted lines). This comparison, Fig. 9, applies to a pseudo-ductile material characterised by Π_N/h = 33.75 (the same as in CC, Section 5.1), with both EH and OH notches. All predictions utilise the pseudo-ductility modified translaminar toughness $\mathcal{J}^{SS}$, which is $1.4\mathcal{G}_{Ic}$.

The accuracy of the s_N and the elastic limit hinges on the precision of K_t^P. Thus, we compare the s_N predictions using K_t^P, from the modified Stowell model (Eq. (19), dotted lines) and FE models (dash-dotted lines) in Fig. 9. For the EH and OH, the FE models yield K_t^P values of 2.03 and 1.52, respectively. However, the modified Stowell model underestimates K_t^P for EH (1.74) while closely matching the FE results for OH. For an equivalent linear elastic material (σ_f = 500 MPa and ε_d = 0), the elastic stress concentration factors, K_t^E, would be 4.24 and 2.58 for EH and OH notches, respectively (Appendix A).

As demonstrated by the s_N from FE models and the modified SEL predictions in Fig. 9, these findings align well with established limits (see Fig. 1). When $R \to \infty$, the expected elastic limit is achieved for both notches, provided that the stress concentration factor K_t^P derived from FE models is used (σ_f/K_t^P values are 246.3 and 328.95 MPa for EH and OH notches, respectively). However, the elastic limit for EH notches is overestimated when K_t^P from the modified Stowell model is used — because the K_t^P is overestimated with Eq. (19) [22].

Bažant's SEL (Fig. 9, solid lines) predicts well the s_N for large specimens, $R \to \infty$, where the average stresses in the failure plane remain elastic ($\sigma_N < \sigma_y$). Nevertheless, Bažant's SEL overestimates the s_N by an average of 11.56 and 7% for EH and OH, respectively, in specimens with $s_N > 1/s_H$, i.e., $\approx R < \ell_{\mathrm{SEL}}(s_H^2 - 1)$, as it does not account for damage due to pseudo-ductility. Conversely, our proposed modifications to the Bažant SEL (Section 2.1) capture s_N behaviour well; within 0.37% for EH and 0.89% for OH, when K_t^P from FE models are used. However, when K_t^P from the modified Stowell model is used, the accuracy of s_N decreases to an average of 6.3% for EH (Fig. 9).

To evaluate the efficacy of our proposed modifications to the scaling laws (Section 2.1) in predicting nominal strength of a wide range of materials, we applied the same procedure to the pseudo-ductile materials included in the DOE (Section 3). The s_N results showcased in Figs. 8 and 10 display a strong "1:1" correlation (R^2) between the FE estimates and the modified size-effect law predictions (Eq. (12)). With the respective R^2 values of 0.992 and 0.990 for EH and OH notches, these values underline the general applicability of the proposed modifications. It is important to note that we used the K_t values from the FE models for this comparison. If the K_t values from the modified Stowell model (Eq. (19)) were used instead, prediction accuracy would remain relatively unchanged for OH but would slightly decrease for EH, reducing the R^2 value to 0.972. This discrepancy can be attributed to the reduced K_t correlation (R^2 = 0.877) between the modified Stowell model predictions and FE results for EH, while OH predictions present an excellent alignment (R^2 = 0.994) [22].

5.3. Generalised behaviour of pseudo-ductile material containing notches

To discern the influence of pseudo-ductility on the s_N, we considered the typical notches (CC, EH and OH) in an infinite plate (R/W = 0). Two pseudo-ductile materials are distinguished by their Π_N/h value ($e_d/(hs_H)$), 0.417 and 33.75 for low and high pseudo-ductility, respectively. A linear elastic material (Π_N/h = 0) is also included to serve as a benchmark.

The functional forms presented in Section 4.1 provide the $\mathcal{J}^{SS}$ (Eq. (16)) and Section 4.2 (Eq. (19)) the K_t^P for any given pseudo-ductile material. It is imperative to highlight that this approach is not exclusive to the configuration with R/W = 0. The influence of finite width is solely accounted for through the geometric correction factor (F) and the corresponding K_t^E. Thus, estimating the s_N for any other R/W ratio involves using the appropriate values of F and K_t^E.

Firstly, we display the normalised size effect [4] behaviour along with the roots of Eq. (10) (Section 2.1.1) for CC specimens in Fig. 11. Fig. 11 showcases the well-established asymptotes of the size effect behaviour (Figs. 1 and 3). By presenting the s_N with normalised material characteristic length (elastic), $\bar{\ell}_M$, pseudo-ductility shifts the s_N by $ln\left(\bar{\mathcal{J}}^{SS}\right)$ on the x-axis. Consequently, the corresponding roots to the yield strength, $ln(1/s_H)$, should also shift, resulting in $\left[(s_H^2 - 1)\bar{\mathcal{J}}^{SS}\right]$ being the critical specimen size. As we have previously demonstrated (Figs. 3 and 7a in [21]), pseudo-ductility exerts a negative impact on specimens below this specimen size and a positive influence above it. The changes to nominal strengths are negligible for materials with low pseudo-ductility (dash-dotted line). However, for materials with high pseudo-ductility (dashed line), s_N decreases below the critical

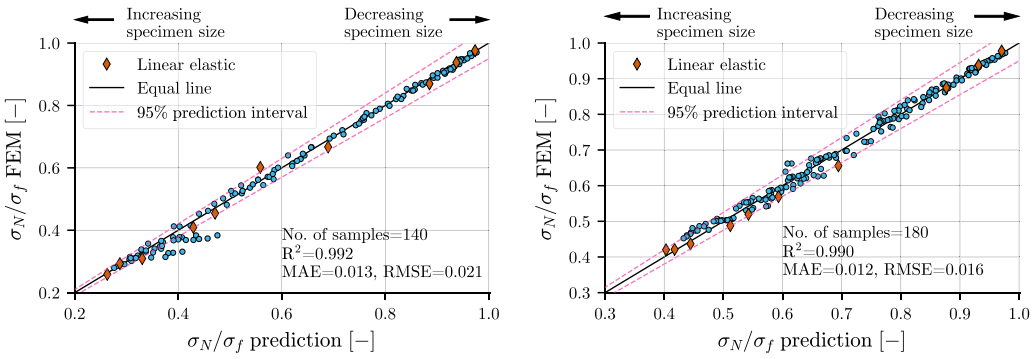

(a) Elliptical-hole (b) Open-hole

Fig. 10. Comparison of notched strengths from FE models and modified nominal strength scaling laws (Section 2.1): A "1:1" correlation analysis. Markers represent FE results (diamonds for linear-elastic, circles for pseudo-ductile). K_t^P from FE models is used.

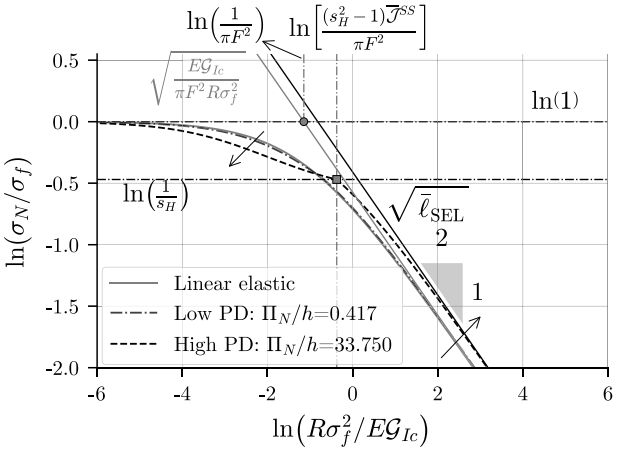

Fig. 11. Comparative analysis of the generalised size-effect behaviour for a CC infinite plate, considering an elastic material and two different pseudo-ductile materials. PD denotes pseudo-ductility, with h values of 0.6 and 0.1 for low and high pseudo-ductile materials, respectively, while $s_H = 1.6$ in both instances. $\overline{\mathcal{J}}^{SS}$ is computed using Eq. (16).

radius but improves above it. With the increase in pseudo-ductility (corresponding to an increase in Π_N/h), the s_N decreases further as the average damage in the failure plane increases for the specimens below the critical specimen size, $\bar{\ell}_{\text{SEL}}\left[(s_H^2-1)\overline{\mathcal{J}}^{SS}\right]$. In contrast, s_N retention increases with increasing pseudo-ductility, as the positive influence of the translaminar toughness is retained when $\sigma_N < \sigma_y$. Further, the elastic limit for any pseudo-ductile material is captured well with the $\sqrt{\bar{\ell}_{\text{SEL}}}$.

Similarly, we illustrate the s_N as a normalised size effect in infinite plates containing EH (Fig. 12a) and OH (Fig. 12b). The nominal strength limits for large specimen size are $ln(1/5)$ and $ln(1/3)$ for EH ($b/R = 1/2$) and OH, respectively ([37], Appendix A). As with CC specimens, pseudo-ductility exerts a positive influence on both notch shapes above the critical radius, $R \gtrapprox \ell_{\text{SEL}}\left[(s_H^2-1)\overline{\mathcal{J}}^{SS}\right]$, but a negative one below it. The influence of the pseudo-ductility is significant, even in the case of low pseudo-ductility, where minor stress redistributions result in substantial nominal strength recovery. For instance, in the low pseudo-ductile material considered ($\Pi_N/h = 0.42$), the K_t is reduced by 16% and 13% for an EH and OH, respectively. This reduction results in a corresponding 10% and 13% nominal strength recovery in EH and OH specimens. In the region of negative influence, EH appears to be more adversely affected than OH, which could be attributed to the increased K_t. As pseudo-ductility is increased, the consequent increase in R/W further reduces the K_t, thereby pushing the elastic limit line upwards. However, altering R/W has a negligible influence in highly pseudo-ductile materials, as changes to K_t^P would be minimal, as is exemplified in Fig. 12b for $\Pi_N/h = 33.75$ with OH.

Leveraging the modifications to SEL (Section 2.1), coupled with our ability to calculate the $\mathcal{J}^{SS}$ and K_t^P for any pseudo-ductile material and notch shape, we plot the nominal strength response for the same three materials across different notch shapes in Fig. 13. The highlighted lines represent the limiting nominal strengths for an OH (black line) and a CC notch (red line). For all notch shapes, pseudo-ductility tends to elevate the surface for $R \gtrapprox \ell_{\text{SEL}}\left[(s_H^2-1)\overline{\mathcal{J}}^{SS}\right]$, while exerting a downward influence below this specimen size.

5.4. Pseudo-ductility and notch-sensitivity

We considered two materials for the analysis of the effect of notch-radius to specimen width: a linear elastic material and a pseudo-ductile material with $\Pi_N/h = 33.75$. Notably, Bažant's SEL [28] presumes consistent geometric ratios between scaled specimens, including a similar damage mode, to asymptotically match the strengths between elastic and plastic limits. Varying the R/W ratio breaches this assumption. We employ distinct SELs for each R/W value to characterise the σ_∞ for a given notch radius. Bažant's SEL for linear elastic specimens (Eq. (3)) and the modified SEL for pseudo-ductile specimens (Eq. (12)) align well with the FE solutions, as illustrated in Fig. 14. As earlier, pseudo-ductility manifests a dual response in this size effect scenario as well, enhancing s_N above a certain notch ratio while adversely affecting it below this value.

6. Discussion

In discussing the implications of our findings, we first provide recommendations to guide future experimental campaigns. Even modest enhancements in K_t due to pseudo-ductility can increase nominal strength retention. For instance, consider the lower range of pseudo-ductility (low pd), as illustrated in Figs. 11 and 12 with $\Pi_N/h = 0.417$, a value closer to current literature [38]. Noticeable nominal strength retention emerges in specimens exceeding the critical notch size. This, however, is contingent upon the condition that the failure strength (σ_f) and fracture energy ($\mathcal{G}_{Ic}$) of the pseudo-ductile laminate is at least equal to those of the linear-elastic (reference) laminate. However, achieving this balance is not straightforward. For instance, owing to the ply thickness influence [11,39], the un-notched strength of thin-ply linear-elastic laminates typically surpasses that of pseudo-ductile laminates. Thus, optimising pseudo-ductility while minimising the un-notched strength reduction is essential for maintaining a favourable balance between these characteristics.

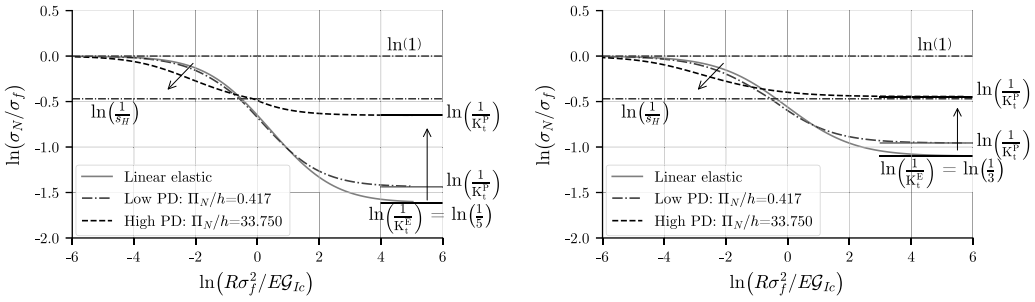

(a) Elliptical-hole (b) Open-hole

Fig. 12. Comparative analysis of the generalised size-effect behaviour for a EH and OH infinite plate, considering an elastic material and two different pseudo-ductile materials. PD denotes pseudo-ductility, with h values of 0.6 and 0.1 for low and high pseudo-ductile materials, respectively, while $s_H = 1.6$ in both instances. The $\bar{\mathcal{J}}^{ss}$ and K_t is computed using Eqs. (16) and (19), respectively.

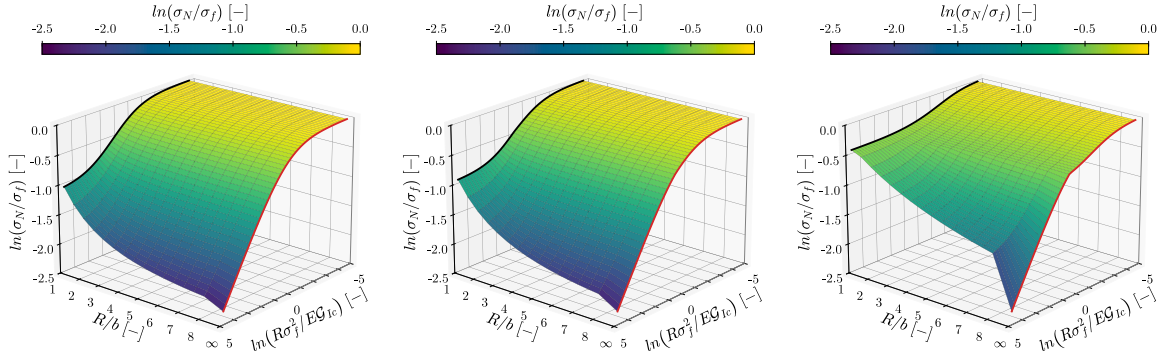

(a) Elastic (b) Low pseudo-ductility (c) High pseudo-ductility

Fig. 13. Generalised size-effect behaviour of pseudo-ductile infinite plate containing wide range of notch shapes (R/b): 1 (Open-hole) and ∞ (centre-crack). Highlighted lines represent the limiting nominal strengths; open-hole (black) and centre-cracked (red).

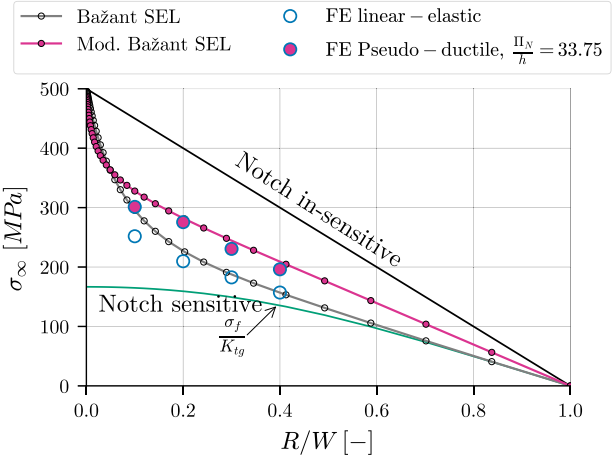

Fig. 14. Open-hole notched (gross-) strength size effect in terms of notch-size ratio (R/W). Validity of the Bažant SEL is dependent on geometric constancy, changing the R/W ration, however, invalidates this condition. Nevertheless, the validity is maintained by extracting the σ_∞ for each R/W ratio using different SELs (Eqs. (3) and (11)).

Secondly, though pseudo-ductility typically manifests as damage post ε_y rather than the metal-like hardening, we hypothesise an intermediate behaviour reminiscent of metals. Recently, for materials following Ramberg–Osgood behaviour [40], Nguyen [25] and Dönmez [41] have rigorously shown the presence of a millimetre-scale fracture process zone and an intermediate asymptotic behaviour bridging the well-established elastic and plastic limits. Drawing parallels from their work, we demonstrate that our approach, as detailed in Section 2.1, is versatile and can be tailored to accommodate different material constitutive behaviours, including those of plastic-hardening materials.

The uniaxial stress–strain behaviour of a plastic-hardening material can be adequately characterised with the Ramberg–Osgood (power-law) [40] as,

$$\varepsilon = \frac{\sigma}{E} + \alpha_p \frac{\sigma_y}{E}\left(\frac{\sigma}{\sigma_y}\right)^n \tag{20}$$

where α_p is an empirical parameter and n is the hardening exponent. Following the approach laid out in Section 4.2 and by Stowell [23], we can first define the plastic stress concentration factor (K_t^P) for a power-law material [22], as,

$$K_t^P = 1 + \left(K_t^E - 1\right)\frac{1 + \alpha_p\left(s_H/K_t^P\right)^{n-1}}{1 + \alpha_p s_H^{n-1}} \tag{21}$$

Subsequently, the secant modulus (E_S) for a power-law material at σ_N is,

$$E_S = \frac{E}{1 + \alpha_p\left(s_H s_N\right)^{n-1}} \tag{22}$$

By substituting Eq. (22) in the modified size effect law (Eq. (11)), the $\bar{\ell}^{-1}_{\text{SEL}}$ is,

$$\bar{\ell}^{-1}_{\text{SEL}} = \frac{1 - s_N^r}{s_N^r - \left(K_t^M\right)^{-r}}\frac{1}{1 + \alpha_p\left(s_H s_N\right)^{n-1}} \quad \text{for } 1/s_H < s_N < 1 \tag{23}$$

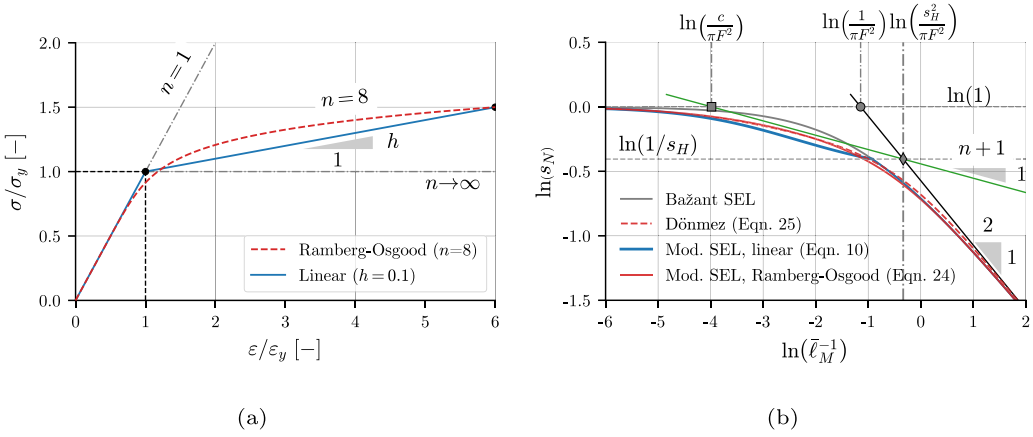

Fig. 15. (a) . Normalised uniaxial stress–strain curves for linear and plastic-hardening materials with $h = 0.1, s_H = 1.5$ and $n = 8$. (b). Normalised size-effect behaviour of CC specimens according to our presented modifications, linear (Eq. (10)), power-law (Eq. (24)) and Eq. (25) presented by Dönmez et al. [41].

where K_t^M is defined according to Eqs. (13) and (21). For a CC specimen ($r = 2$ and $K_t^M \to \infty$), the size effect law (Eq. (23)) can be expressed as,

$$\bar{\ell}_{\text{SEL}}^{-1} = \frac{1 - s_N^2}{s_N^2} \frac{1}{1 + \alpha_p \left(s_H s_N\right)^{n-1}} \quad \text{for } 1/s_H < s_N < 1 \tag{24}$$

Recently, Nguyen [25] investigated the strength scaling laws associated with specimens containing a sharp crack in elasto-plastic materials following the power-law (Eq. (20)). Further, Dönmez [41], in a related development, proposed the subsequent size effect law (adapted with the notation of this paper),

$$s_N = \left[\left(1 + \bar{\ell}_{\text{SEL}}^{-1}/c\right)^{\sqrt{2/(n+1)}} + \left(\bar{\ell}_{\text{SEL}}^{-1}\right)^{\sqrt{(n+1)/2}}\right]^{-1/\sqrt{2(n+1)}} \tag{25}$$

This equation adheres to the well-known strength limits of a CC specimen: $s_N = 1$ for very small specimens $\left(\bar{\ell}_{\text{SEL}}^{-1} \to 0\right)$ and $s_N = \left(\bar{\ell}_{\text{SEL}}\right)^{1/2}$ for very large specimens $\left(\bar{\ell}_{\text{SEL}}^{-1} \to \infty\right)$. Additionally in Eq. (25), there exists an intermediate asymptote, $s_N = (c\bar{\ell}_{\text{SEL}})^{1/(n+1)}$, for specimen sizes in the region where $1/c\pi < \bar{\ell}_{\text{SEL}}^{-1} < s_H^2/\pi$.

Using the same arbitrary pseudo-ductile material from our analysis of the proposed modifications in Section 2.1.1 – $s_H = 1.5$ and $h = 0.1$, together with a nearly equivalent plastic-hardening material (Eq. (20)) with $n = 8$, we demonstrate the behaviour of Eqs. (24) and (25) alongside Eqs. (9) and (10). The stress–strain curves for both the considered materials, in their normalised form, are shown in Fig. 15a. Fig. 15b presents the s_N values for both materials, across $\bar{\ell}_{\text{M}}$ values ranging from 10^{-3} to 10^3. To fit the SEL (Eq. (25)), an additional parameter, $c = s_H^{(1-n)} = 0.0585$, is chosen to ensure that the two asymptotes (intermediate and large-size asymptote) intersect at the yield strength, or $s_N = s_H^{-1}$. Fig. 15b clearly demonstrates that our proposed modifications closely align with the comprehensive treatment recently proposed by Nguyen et al. [25] and Dönmez et al. [41].

7. Conclusions

This work proposed modifications to nominal strength scaling laws to account for the effects of pseudo-ductility. Our previous research [21,22] demonstrated that the conventional scaling laws (Bažant SEL), although helpful, fall short of capturing the negative effect displayed by the notched pseudo-ductile materials for specimen sizes below a critical specimen size, $R < \ell_{\text{SEL}}\left[(s_H^2 - 1)\overline{\mathcal{J}}^{SS}\right]$. We proposed modifications to these scaling laws, drawing on the ideas of Nguyen et al. [25] and Stowell [23].

It was necessary to calculate the altered translaminar toughness for any pseudo-ductile material to implement these modifications, as it is influenced by pseudo-ductility. Our non-dimensional analysis facilitated the identification of a functional form that captures this increment of translaminar toughness well.

The effectiveness of these modifications is emphasised by their ability to predict the nominal strengths for a wide range of pseudo-ductile materials. A "1:1" correlation coefficient (R^2) of 0.997, 0.992, and 0.990 was achieved between the predicted and FE estimates for CC, EH, and OH shapes, respectively. Utilising these modified scaling laws, we also illustrated the influence of pseudo-ductility on nominal strength across various notch shapes, from CC to OH, and the size effect on nominal strength in terms of the notch size ratio.

Our findings highlight the potential benefits of pseudo-ductility in improving the notched strength recovery, achieved through enhanced translaminar toughness and reduced stress concentration factor. However, a critical caveat emerges from this study: since pseudo-ductility is based on promoting non-recoverable sub-critical damage mechanisms, it can have an adverse effect on specimens falling below a critical specimen size. This highlights the necessity for careful consideration when applying pseudo-ductile materials, particularly for small-scale specimens. Moreover, the modifications we proposed to Bažant SEL can help quickly characterise the size effect behaviour.

CRediT authorship contribution statement

A. Subramani: Conceptualization, Methodology, Software, Visualization, Writing – original draft, Writing – review & editing. **P. Maimí:** Conceptualization, Funding acquisition, Resources, Supervision, Validation, Writing – review & editing. **J. Costa:** Funding acquisition, Resources, Supervision, Writing – review & editing.

Declaration of competing interest

The authors declare that they have no known competing financial interests or personal relationships that could have appeared to influence the work reported in this paper.

Data availability

No data was used for the research described in the article.

Acknowledgements

The authors acknowledge the funding and support of Ministerio de Ciencia, Innovación *y* Universidades for the project *En pos de materiales compuestos de fibra larga híbridos, bio-basados y sostenibles para aplicaciones estructurales* (SUBHYCO) (PID2021-126989OB-I00). Anbazhagan Subramani acknowledges the financial support of the Universitat de

Girona for INV309_2019 and would also like to thank Universitat de Girona and Santander Universidades for the financial resources provided through *Personal Investigador en formació* (IF_UDG), 2020. Open Access funding provided thanks to the CRUE-CSIC agreement with Elsevier.

Appendix A. Elastic stress concentration factor equations

The equations for the elastic stress concentration factors, defined in terms of nominal stress (net-section stress), for an open-hole and an elliptical-hole in the plate centre are [37],

$$\left(K_t^E\right)_{\mathrm{OH}} = 2 + 0.284\left(1-\frac{R}{W}\right) - 0.600\left(1-\frac{R}{W}\right)^2 + 1.32\left(1-\frac{R}{W}\right)^3 \quad \text{(A.1)}$$

$$\left(K_t^E\right)_{\mathrm{EH}} = C_1 + C_2\left(\frac{R}{W}\right) + C_3\left(\frac{R}{W}\right)^2 + C_4\left(\frac{R}{W}\right)^3 \quad \text{(A.2)}$$

while $1.0 \le R/b \le 8.0$, the coefficients are,

$$C_1 = 1.109 - 0.188\sqrt{R/b} + 2.086R/b$$
$$C_2 = -0.486 + 0.213\sqrt{R/b} - 2.588R/b$$
$$C_3 = 3.816 - 5.510\sqrt{R/b} + 4.638R/b$$
$$C_4 = -2.438 + 5.485\sqrt{R/b} - 4.126R/b$$

The nominal and gross stress concentration factors are related through,

$$K_{tg} = K_t\left(1-\frac{R}{W}\right)^{-1} \quad \text{(A.3)}$$

Appendix B. Finite width correction factor

The finite width correction factor for all the considered geometries is given by [29],

$$F = \left[1 - 0.025\left(\frac{R}{W}\right)^2 + 0.06\left(\frac{R}{W}\right)^4\right]\sqrt{\sec\left(\frac{\pi}{2}\frac{R}{W}\right)} \quad \text{(B.1)}$$

where R/W is the ratio of notch radius to specimen width.

Appendix C. Functional form identification for translaminar toughness of pseudo-ductile materials

Our previous work [21], utilising the same DOE (Fig. 4), suggested a near-linear relationship for $\bar{\mathcal{J}}^{SS}(\varepsilon_d)$, which can be conveniently approximated by,

$$\bar{\mathcal{J}}^{SS} \approx 1 + m\varepsilon_d \quad \text{(C.1)}$$

Further, the non-dimensional analysis presented in Eq. (15) suggests that the slope, m, should also be depend on the strength ratio, $s_H (= \sigma_f/\sigma_y)$. Rearranging Eq. (C.1), we obtain,

$$\frac{\bar{\mathcal{J}}^{SS} - 1}{\varepsilon_d} \approx m \quad \text{(C.2)}$$

By examining m versus s_H (see Fig. C.16a), we can establish a fitting equation for m that encompasses both the influential non-dimensional variables ε_d and s_H. Fitting the FE data to Eq. (C.2) leads to a satisfactory approximation of the form,

$$m = B\left(\frac{1}{s_H}\right)^a\left(s_H - 1\right) \quad \text{(C.3)}$$

By substituting the coefficients (B and a) from Eq. (C.3) to Eq. (C.1), the $\bar{\mathcal{J}}^{SS}$ can be represented as Eq. (16).

Alternatively, from the perspective of strain energy, Zehnder [35] proposed the steady-state energy release rate ($\mathcal{J}^{SS}$) for elastic–plastic materials, to be of the form,

$$\mathcal{J}^{SS} = \mathcal{G}_{Ic} + R_0\Phi_p \quad \text{(C.4)}$$

where R_0 is the plastic zone size and Φ_p is the energy per unit volume of material associated with unloading. For the idealised pseudo-ductile material, Fig. 2b, the unloading phase ($\sigma > \sigma_y$) signifies a damaged material with a reduced elastic modulus that reaches the origin. Therefore, the energy under the unloading curve, Φ_p, can be expressed as,

$$\Phi_p = \frac{\sigma_y^2}{2E}\left(\frac{E}{H} - 1\right)\left(\frac{\sigma_f}{\sigma_y} - 1\right) \quad \text{(C.5)}$$

Substituting Eq. (C.5) and the first-order plastic zone estimate, the Irwin length $R_0 = \left(E\mathcal{G}_{Ic}\right)/\left(\pi\sigma_f^2\right)$, into Eq. (C.4), results in Eq. (17).

Appendix D. Derivation of modified size effect law for centre-cracked notch

We define the inverse of the normalised failure process zone (FPZ) length, $\bar{\ell}_{\mathrm{SEL}}$, as x for convenience,

$$x = \bar{\ell}_{\mathrm{SEL}}^{-1} = \frac{RF^2\sigma_f^2}{E\mathcal{J}^{SS}} \quad \text{(D.1)}$$

For a pseudo-ductile material described by Eq. (6), substituting the pristine materials' elastic modulus in (E) in Eq. (D.1) with the secant modulus (E_s) results in $\bar{\ell}_{\mathrm{SEL}}$ within the "yielding" region ($1/s_H < s_N < 1$). Therefore, when $\sigma_i = \sigma_N$,

$$\bar{\ell}_{\mathrm{SEL}}^{-1} = \frac{RF^2\sigma_f^2\left(\sigma_N - (1-h)\sigma_y\right)}{E\mathcal{J}^{SS}h\sigma_N} = \frac{\sigma_N - (1-h)\sigma_y}{h\sigma_N\bar{\ell}_{\mathrm{SEL}}^{-1}} \quad \text{(D.2)}$$

where, $\mathcal{J}^{SS}$ is the translaminar toughness of the pseudo-ductile material.

According to LEFM, the s_N size-effect relationship for a CC pseudo-ductile specimen is given by Eq. (9). Through Eq. (D.1) it can be conveniently represented as,

$$\left(s_N\right)_{\mathrm{LEFM}} = \sqrt{\frac{1}{x}} \quad \text{(D.3)}$$

Now, we can extend the LEFM size effect to accommodate the effective modulus modification by replacing $\bar{\ell}_{\mathrm{SEL}}$ in Eq. (D.3) with $\bar{\ell}_{\mathrm{SEL}^*}$ (Eq. (8)) and subsequently solving for σ_N (in the region $1/s_H < s_N < 1$):

$$\sigma_N = \frac{1}{2}\left(\sigma_y - h\sigma_y + \sqrt{\frac{4Eh\mathcal{J}^{SS}}{RF^2} + (h-1)^2\sigma_y^2}\right) \quad \text{(D.4)}$$

By re-arranging Eq. (D.4) and normalising by σ_f,

$$(s_N)_{\mathrm{LEFM}} = \frac{\sigma_N}{\sigma_f} = \frac{1-h}{2s_H} + \sqrt{\frac{h}{\bar{\ell}_{\mathrm{SEL}}^{-1}} + \left(\frac{h-1}{2s_H}\right)^2} \quad \text{(D.5)}$$

In a similar vein, we apply the secant modulus modification to Bažant SEL (Eq. (3)). Firstly, for a CC notch configuration ($K_t = \infty$ and $r = 2$) the SEL can be succinctly expressed using x (Eq. (D.1)) as,

$$\left(s_N\right)_{\mathrm{SEL}} = \sqrt{\frac{\bar{\ell}_{\mathrm{SEL}}}{1+\bar{\ell}_{\mathrm{SEL}}}} = \sqrt{\frac{1/x}{1+1/x}} = \sqrt{\frac{1}{1+x}} \quad \text{(D.6)}$$

By replacing $\bar{\ell}_{SEL}$ in Eq. (D.6) with $\bar{\ell}_{\mathrm{SEL}^*}$ (Eq. (D.2)) and solving for σ_N within the region $1/s_H < s_N < 1$,

$$\sigma_N = \frac{RF^2\sigma_f^2\sigma_y(1-h) + \sqrt{4Eh\mathcal{J}^{SS}\sigma_f^2\left(Eh\mathcal{J}^{SS} + RF^2\sigma_f^2\right) + \left[RF^2\sigma_f^2\sigma_y(-1+h)\right]^2}}{2\left(Eh\mathcal{J}^{SS} + RF^2\sigma_f^2\right)} \quad \text{(D.7)}$$

Re-arranging Eq. (D.7) and normalising by σ_f, gives Eq. (10).

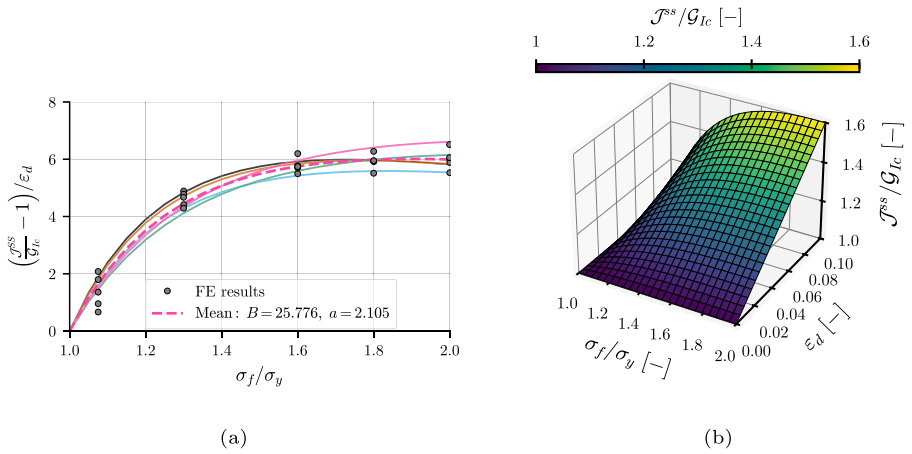

Fig. C.16. Translaminar toughness of pseudo-ductile materials. (a). Determination of fitting coefficients for Eq. (C.3) (b). Surface plot of the fitted translaminar toughness function (Eq. (16)) with the dependencies.

Appendix E. Coefficient of determination of the modified size-effect law

To assess the effectiveness of the proposed modifications outlined in Section 2.1, we illustrate the "1:1" correlation between FE and predicted s_N values for all three notch types (CC, EH and OH) in Figs. 8 and 10. These plots also contain other metrics, such as the total number of evaluated specimens, coefficient of determination (R^2), Mean Average Error (MAE), and Root Mean Square Error (RMSE) for a comprehensive evaluation. All notch radii in the intermediate region are considered, defined by $R < \ell_{\text{SEL}}\left[(s_H^2 - 1)\overline{\mathcal{J}}^{SS}\right]$, totalling 100 samples in each notch. Beyond this region, we selected only a subset of radii as the influence of pseudo-ductility can be solely characterised using the appropriate translaminar toughness $\left(\overline{\mathcal{J}}^{SS}\right)$ and K_t^{PD}, see Section 2.1.

References

[1] Z.P. Bazant, I.M. Daniel, Z. Li, Size effect and fracture characteristics of composite laminates, J. Eng. Mater. Technol. 118 (1996) 317–324.

[2] B. Green, M. Wisnom, S. Hallett, An experimental investigation into the tensile strength scaling of notched composites, Composites A 38 (3) (2007) 867–878.

[3] X. Xu, M.R. Wisnom, Y. Mahadik, S.R. Hallett, An experimental investigation into size effects in quasi-isotropic carbon/epoxy laminates with sharp and blunt notches, Compos. Sci. Technol. 100 (2014) 220–227.

[4] Z.P. Bažant, Scaling theory for quasibrittle structural failure, Proc. Natl. Acad. Sci. 101 (37) (2004) 13400–13407.

[5] P.P. Camanho, P. Maimí, C. Dávila, Prediction of size effects in notched laminates using continuum damage mechanics, Compos. Sci. Technol. 67 (13) (2007) 2715–2727.

[6] P. Maimí, D. Trias, E. González, J. Renart, Nominal strength of quasi-brittle open hole specimens, Compos. Sci. Technol. 72 (10) (2012) 1203–1208.

[7] P. Maimí, E.V. González, N. Gascons, L. Ripoll, Size effect law and critical distance theories to predict the nominal strength of quasibrittle structures, Appl. Mech. Rev. 65 (2) (2013).

[8] P. Lagace, Static Tensile Fracture of Graphite/epoxy (Ph.D. thesis), Technology Laboratory for Advanced Composites, Department of Aeronautics and Astronautics, Massachusetts Institute of Technology, 1986.

[9] A. Nijs, M. Selezneva, Y. Swolfs, N. Hirano, I. Taketa, T. Karaki, I. Verpoest, L. Gorbatikh, Notch-sensitivity of hybrid carbon-fibre/self-reinforced polypropylene composites, Compos. Sci. Technol. 200 (2020) 108422.

[10] A. Arteiro, Structural mechanics of thin-ply laminated composites (Ph.D. thesis), Universidade do Porto (Portugal), 2016.

[11] R. Amacher, J. Cugnoni, J. Botsis, L. Sorensen, W. Smith, C. Dransfeld, Thin ply composites: Experimental characterization and modeling of size-effects, Compos. Sci. Technol. 101 (2014) 121–132.

[12] G. Guillamet, A. Turon, J. Costa, J. Renart, P. Linde, J. Mayugo, Damage occurrence at edges of non-crimp-fabric thin-ply laminates under off-axis uniaxial loading, Compos. Sci. Technol. 98 (2014) 44–50.

[13] Y. Swolfs, L. Gorbatikh, I. Verpoest, Fibre hybridisation in polymer composites: A review, Composites A 67 (2014) 181–200.

[14] G. Czél, M.R. Wisnom, Demonstration of pseudo-ductility in high performance glass/epoxy composites by hybridisation with thin-ply carbon prepreg, Composites A 52 (2013) 23–30.

[15] J. Fuller, M. Wisnom, Pseudo-ductility and damage suppression in thin ply CFRP angle-ply laminates, Composites A 69 (2015) 64–71.

[16] M.R. Wisnom, G. Czél, Y. Swolfs, M. Jalalvand, L. Gorbatikh, I. Verpoest, Hybrid effects in thin ply carbon/glass unidirectional laminates: Accurate experimental determination and prediction, Composites A 88 (2016) 131–139.

[17] M. Fotouhi, M. Jalalvand, M.R. Wisnom, High performance quasi-isotropic thin-ply carbon/glass hybrid composites with pseudo-ductile behaviour in all fibre orientations, Compos. Sci. Technol. 152 (2017) 101–110.

[18] G. Czél, M. Jalalvand, M. Fotouhi, M.L. Longana, O.J. Nixon-Pearson, M.R. Wisnom, Pseudo-ductility and reduced notch sensitivity in multi-directional all-carbon/epoxy thin-ply hybrid composites, Composites A 104 (2018) 151–164.

[19] M. Fotouhi, M. Jalalvand, M.R. Wisnom, Notch insensitive orientation-dispersed pseudo-ductile thin-ply carbon/glass hybrid laminates, Composites A 110 (2018) 29–44.

[20] S. Sapozhnikov, S. Lomov, Y. Swolfs, V. Carvelli, Deformation and failure of pseudo-ductile quasi-isotropic all-carbon hybrid FRPS with an open hole under tension, Composites B 237 (2022) 109870.

[21] A. Subramani, P. Maimi, J. Costa, On How Pseudo-Ductility Modifies the Translaminar Fracture Toughness of Composites and the Nominal Strength of Centre-Cracked Specimens, Elsevier, 2023, Submitted for publication.

[22] A. Subramani, P. Maimí, J. Guerrero, J. Costa, Nominal strength of notched pseudo-ductile specimens, Theor. Appl. Fract. Mech. (2023) 104120.

[23] E.Z. Stowell, Stress and Strain Concentration At a Circular Hole in an Infinite Plate, National Advisory Committee for Aeronautics, Washington, DC, 1950.

[24] H. Hardrath, L. Ohman, A Study of Elastic and Plastic Stress Concentration Factors Due to Notches and Fillets in Flat Plates, Technical Report, 1953, National Advisory Committee for Aeronautics, 1953.

[25] H.T. Nguyen, A.A. Dönmez, Z.P. Bažant, Structural strength scaling law for fracture of plastic-hardening metals and testing of fracture properties, Extreme Mech. Lett. 43 (2021) 101141.

[26] J.F. Mandell, S.-S. Wang, F.J. McGarry, The extension of crack tip damage zones in fiber reinforced plastic laminates, J. Compos. Mater. 9 (3) (1975) 266–287.

[27] G.R. Irwin, Analysis of stresses and strains near the end of a crack traversing a plate, ASME J. Appl. Mech. 24 (1957) 361–364.

[28] Z.P. Bažant, J. Planas, Fracture and Size Effect in Concrete and Other Quasibrittle Materials, Routledge, 2019.

[29] H. Tada, P.C. Paris, G.R. Irwin, the Stress Analysis of Cracks Handbook, Third Ed., ASME Press, 2000.

[30] D.E. Sommer, S.G. Kravchenko, W.B. Avery, R.B. Pipes, Mechanisms of notch insensitivity in long-fiber discontinuous, prepreg platelet compression molded composites, Composites A 162 (2022) 107133.

[31] E.J. Barbero, Finite Element Analysis of Composite Materials using Abaqus™, vol. 2103, CRC press Boca Raton, 2013.

[32] W. Brocks, A. Cornec, I. Scheider, 3.03 - Computational aspects of nonlinear fracture mechanics, in: I. Milne, R. Ritchie, B. Karihaloo (Eds.), Comprehensive Structural Integrity, Pergamon, Oxford, 2003, pp. 127–209.

[33] C. Chen, N.A. Fleck, T. Lu, The mode I crack growth resistance of metallic foams, J. Mech. Phys. Solids 49 (2) (2001) 231–259.

[34] V. Tvergaard, J.W. Hutchinson, The relation between crack growth resistance and fracture process parameters in elastic-plastic solids, J. Mech. Phys. Solids 40 (6) (1992) 1377–1397.

[35] A. Zehnder, C. Hui, A simple model relating crack growth resistance to fracture process parameters in elastic-plastic solids, Scripta Materialia 42 (10) (2000) 1001–1005.

[36] F. Herbert, A study of elastic and plastic stress concentration factors due to notches and fillets in flat plates, Ann. Rep.-Natl. Advis. Comm. Aeronaut. 103 (2) (1955) 213.
[37] W.D. Pilkey, D.F. Pilkey, Z. Bi, Peterson's Stress Concentration Factors, John Wiley & Sons, 2020.
[38] G. Czél, M. Jalalvand, M. Fotouhi, M.L. Longana, O.J. Nixon-Pearson, M.R. Wisnom, Pseudo-ductility and reduced notch sensitivity in multi-directional all-carbon/epoxy thin-ply hybrid composites, Composites A 104 (2018) 151–164.
[39] C. Furtado, A. Arteiro, P. Linde, B. Wardle, P. Camanho, Is there a ply thickness effect on the mode I intralaminar fracture toughness of composite laminates? Theor. Appl. Fract. Mech. 107 (2020) 102473.
[40] W. Ramberg, W.R. Osgood, Description of Stress-Strain Curves by Three Parameters, Technical Report, 1943.
[41] A.A. Dönmez, H.T. Nguyen, H. Xu, Z.P. Bažant, Crack-parallel stress effect on fracture energy of plastic hardening polycrystalline metal identified from gap test scaling, J. Mech. Phys. Solids 173 (2023) 105222.